Discrete element modelling of missile impacts on a reinforced concrete target

Wenjie Shiu, Frédéric Victor Donzé and Laurent Daudeville*

Laboratoire Sols Solides Structures,
Joseph Fourier University,
B.P. 53, 38041 Grenoble Cedex 9, France
E-mail: wen-jie.shiu@hmg.inpg.fr
E-mail: frederic.donze@hmg.inpg.fr E-mail: laurent.daudeville@ujf-grenoble.fr
*Corresponding author

Abstract: A three-dimensional Discrete Element Method (DEM) is used to study the penetration and perforation process of a concrete target subjected to rigid flat-nose-shaped missile impacts. The evolution of the missile velocity is compared with real test cases made by the French Atomic Energy Agency (CEA) and the French Electrical Power Company (EDF). The perforation limits observed in the experimental data are well predicted by the three-dimensional discrete element model. Parametric studies are then carried out to show the respective roles of the mechanical components, such as the dependence of the perforation process on the percentage of reinforcement.

Keywords: DEM; discrete element method; reinforced concrete; missile impact; scabbing; penetration.

Reference to this paper should be made as follows: Shiu, W., Donzé, F.V. and Daudeville, L. (2009) 'Discrete element modelling of missile impacts on a reinforced concrete target', *Int. J. Computer Applications in Technology*, Vol. 34, No. 1, pp.33–41.

Biographical notes: Wenjie Shiu received his PhD in Structural Engineering from Joseph Fourier University in 2008. He is currently post-doc and participates to the development of Yade, an open source discrete element code for the analysis of structures under impacts

Frédéric Victor Donzé is Professor at Joseph Fourier University, Grenoble. He was involved in several developments of numerical approaches based on the discrete element method and supervises the development of the open source software Yade.

Laurent Daudeville is Professor at Joseph Fourier University, Grenoble. His research activities have included studies of modelling of damage in structures, various problems on different materials such as laminated carbon-epoxy composites, wood, glass and concrete. His current research activities concern the modelling of concrete structures under impacts.

These three people work with a team whose activity deals with the modelling of concrete structures under impacts.

1 Introduction

The design of concrete structures to protect against severe impacts requires models with high predicting capabilities. These models consider four major quantities (Degen, 1980; Hughes, 1984), which measure the local impact effects on a concrete structure: the penetration depth, the scabbing, the perforation and the ballistic limits. The penetration depth is the distance a projectile penetrates a thick concrete target without resulting in perforation and scabbing. The perforation or scabbing limit is the minimum thickness of the target to prevent perforation or scabbing and the ballistic limit is the minimum initial impact velocity to perforate the target.

Many of the available protective design guidelines recommend the use of empirical approaches for the assessment of penetration, scabbing and perforation (Li et al., 2006). For instance, the CEA–EDF formula (Berriaud et al., 1978) is a perforation limit criterion based on a series of weight drops and air gun tests to develop reliable predictions on the ballistic performance of reinforced concrete slabs undergoing a missile impact.

The available empirical formulae were mainly developed by data-fitting of test results. Consistent results over the ordnance velocity range were observed for the different approaches, and the main differences begin at the lower impact velocities in non-military applications (Williams, 1994). However, some of them are

dimensionally non-homogeneous and thus unit-dependent, which provide little physical meaning of the local impact event (Li and Tong, 2003). In addition, the application range of the formulae depends on the tests performed. Theoretical and analytical approaches, such as numerical studies, are also conducted to overcome the shortcomings of these empirical formulae to get a better understanding of the problem.

The Discrete Element Method (DEM) (Cundall and Starck, 1979), which is an alternative numerical method to continuum-type methods, is used here to study the behaviour of concrete structures subjected to rigid impacts. This method does not rely upon any assumption about where and how a crack or several cracks occur and propagate, since the medium is naturally discontinuous and is very well adapted to dynamic problems, when a transition from the solid state to a granular flow regime is observed.

Nevertheless, when a DEM model is used, the issue of the modelling scale has to be addressed: the DEM is well adapted to the modelling of granular material, where an element represents a grain (Cundall and Strack, 1979; Iwashita and Oda, 2000). Numerous authors have also used the DEM to simulate cohesive geomaterials such as concrete, at the heterogeneity scale (Potapov et al., 1995; Potyondy et al., 1996), i.e., the size of an element is in the order of the size of the biggest heterogeneity. This approach gives a better understanding of concrete fracture, but makes the modelling of real structures difficult because of the computational cost. Another way to use the DEM consists in using a higher-scale model, which considers that the whole collection of elements must reproduce the macroscopic behaviour of concrete. Such an approach was mainly developed in 2D (Magnier and Donzé, 1998; Meguro and Hakuno, 1989) or in 3D with a regular assembly of discrete elements (Riera and Iturrioz, 1998).

To get more insight into the perforation process of a concrete slab subjected to rigid flat-nose-shaped missile impacts, a real three-dimensional reinforced concrete structure has been simulated with the DEM. In the following work, the prediction of the missile trajectory was compared with experimental data. Before this last step was possible, the model had to go through a validation process through quasi-static uniaxial tests, which allowed the minimum definition of a parameter identification process (Donzé et al., 1999; Hentz et al., 2004a, 2004b); thus, the modelling scale imposed by the available computing power is controlled, and the simulations are capable of predicting the observed perforation limits.

This three-dimensional approach can predict the penetration depth or the perforation residual velocity of the missile. Moreover, the influence of the reinforcement ratio on the perforation process has been analysed since the available empirical formulae either neglect this parameter or take it into account in a simplified way. The nose shape effect of missiles was investigated in Shiu et al. (2008a).

2 The DEM model

Following the impact simulations (Magnier and Donzé, 1998; Camborde et al., 2000), in which the SDEC code was used (Donzé and Magnier, 1997), the potentiality of the PFC^{3D} code (2003) to simulate real test cases is now investigated.

In the PFC^{3D} code, the discrete elements are spherical and interact with a force–displacement type law, (see equation (1a)). The equations of motion applied to each element are defined by equations (1b) and (1c).

$$F_i = K_i U_i \tag{1a}$$

$$F_i = m(\ddot{x}_i - g_i) \quad \text{(translational motion)} \tag{1b}$$

$$M_i = I\dot{\omega}_i \quad \text{(rotational motion)} \tag{1c}$$

where F_i is the ith component of the contact force, K_i the stiffness associated to each element, with *kn* in the normal direction and *ks* in the tangent direction, U_i is the overlap between two elements in contact, m is the mass of each element, $\ddot{x}$ and $\dot{\omega}$ are the translational acceleration and rotational acceleration, respectively, g is the gravitational acceleration, M_i is the resultant moment acting on each element and I is the moment of inertia. During the calculation cycle, the force–displacement law (equation (1a)) is calculated first, then the new element's position will be updated by the law of motion (equations (1b) and (1c)). Note that more information about the formulation of PFC^{3D} can be found in PFC^{3D} (2003). A more refined constitutive model for penetration is available in Shiu et al. (2008b).

PFC^{3D} provides two ways of formulating the interaction between two elements: the contact and parallel bonds. Because the present objective was to simulate concrete, which is a frictional-cohesive material, the parallel bond has been chosen for the numerical modelling, since it can transfer both the contact force and moment between two elements in contact. The parallel bond is to be treated as glue lying on a finite circular cross-section between two elements. To form a parallel bond, its stiffness and yield stress should be defined before the calculation as well. Thus, new intrinsic parameters are involved, such as pb_kn, pb_ks, pb_nstrength, and pb_sstrength, which are normal and tangent stiffness, and normal and shear yield stress, respectively. The stress that acts on the parallel bond was calculated via the beam theory (see Figure 1). If either of the maximum stresses exceeds its corresponding bond resistance, the parallel bond breaks. Thus, a simple elastic-brittle behaviour was used here. The transferring force in a parallel bond is described in equation (2) by replacing the stiffness terms by pb_kn and pb_ks. The moment transfers between two bonded elements is calculated by

$$\overline{M}_i^n = \overline{k}^s J \Delta\theta^n \tag{2a}$$

$$\overline{M}_i^s = \overline{k}^n I \Delta\theta^s \tag{2b}$$

where $\overline{M}_i^n$ and $\overline{M}_i^s$ are the normal and tangent generalised moments, respectively, $\overline{k}^n$ and $\overline{k}^s$ are the normal and the tangent stiffnesses of the parallel bond, respectively, J is the polar moment of the disk's cross-section, I is the moment of inertia of the disk's cross-section, $\Delta\theta^n$ and $\Delta\theta^s$ are the normal and the tangent relative angular rotation between two elements in contact. Furthermore, when a parallel bond exists between two elements, slip may occur between these bonded elements.

Energy dissipation was also used in our numerical model. The energy involved between two interacting elements is dissipated through frictional sliding for which a Coulomb friction coefficient μ is defined. Moreover, a local non-viscous damping is available in PFC^{3D}, where the damping force is put together with the equation of motion such that,

$$F_{(i)} + F_{(i)}^d = M_{(i)} A_{(i)}; \tag{3}$$

where $F(i)$, $M(i)$, and $A(i)$ are the generalised force, mass and acceleration components, respectively, and $F_{(i)}^d$ is the damping force

$$F_{(i)}^d = -\alpha \left| F_{(i)} \right| \text{sign}(V_{(i)});$$
$$\text{sign}(y) = \begin{cases} +1, & \text{if } y > 0; \\ -1, & \text{if } y < 0; \\ 0, & \text{if } y = 0 \end{cases} \tag{4}$$

where α is the numerical damping (the detailed description can be found in the PFC^{3D} manual). After some pre-process numerical simulation tests, the numerical damping factor is set to 0.15 and 0.05 for the concrete element and the reinforcement element, respectively.

Figure 1 Force and moment components of a parallel bond cohesive interaction

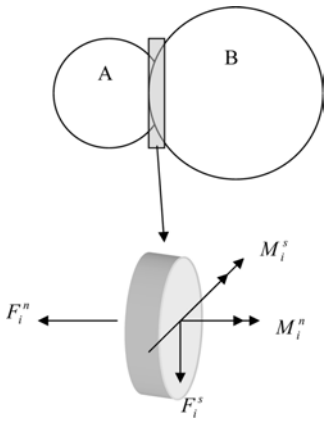

2.1 Local parameters identification process

The goal is to model a structure, in which some of the macroscopic material properties (Young's modulus, Poisson's ratio, tensile and compressive strengths) are known. The structure's geometry is discretised with a collection of discrete elements. To each of these elements, a set of local parameters is assigned so that the macroscopic behaviour of this collection is representative of the real material. This procedure is fully described in Hentz et al. (2004a) and is based on the simulation of quasi-static uniaxial compression/traction tests.

A tri-axial test model is pre-developed in PFC^{3D} and for a standard-sized specimen:

- A compact, polydisperse discrete element collection is generated.
- An elastic compression test is run with local elastic parameters given by the 'macro–micro' relations.
- Compressive and tensile rupture axial tests are simulated to deduce the remaining local parameters.

By performing these tests, the local parameters *kn*, *ks*, pb_kn, pb_ks, pb_nstrength, pb_sstrength are set such that the global mechanical properties of the collection of discrete elements are as close as possible to those of a concrete with a 35 GPa Young's modulus and a 30 MPa compressive strength.

Then, when simulating the first impact test, some readjustments were needed to fit the experimental data set. This readjustment procedure was performed only once (in the D22 impact test chosen as the reference test case), and the exact same set of parameters was used in all subsequent impact test cases to demonstrate the predicting capability of the method. The input numerical data are given in Tables 1 and 2.

Table 1 Parameters used in the model for the concrete (nomenclature of *PFC^{3D}* is used)

Parallel-bond normal stiffness Pb_kn (Pa/m)	70×10^9
Parallel-bond shear stiffness Pb_ks (Pa/m)	14×10^9
Parallel-bond maximum normal stress Pb_nstrength (MPa)	230
Parallel-bond maximum shear stress Pb_sstrength (MPa)	23
Numerical damping α	0.05
Friction coefficient μ	0.3
Density ρ_c (kg/m^3)	2500
Young's modulus E_c (GPa)	35

Table 2 Parameters used in the model for the steel reinforcement (nomenclature of *PFC^{3D}* is used)

Parallel-bond normal stiffness Pb_kn (N/m)	21000×10^9
Parallel-bond shear stiffness Pb_ks (N/m)	5250×10^9
Parallel-bond maximum normal stress Pb_nstrength (MPa)	3500
Parallel-bond maximum shear stress Pb_sstrength (MPa)	1250
Numerical damping α	0.15
Friction coefficient μ	0.3
Density ρ_c (kg/m^3)	28,000
Young's modulus E_s (GPa)	210

2.2 Introducing reinforcement

As in work by other authors (Meguro and Hakuno, 1989; Masuya et al., 1994), reinforcement bars are represented as lines of elements placed next to one another, which have the same diameter as the diameter of the rebar. In the CEA–EDF test data, there are four reinforcement layers placed at equal distances in the concrete target slab. The same geometrical configuration is used in the numerical model and parallel bonds are used between the rebar elements.

In terms of the local behaviour of the reinforcement elements, a simplified model is used here: instead of the elastic–plastic behaviour observed in steel rebars only an elastic-brittle behaviour is considered, because plasticity is not defined in PFC^{3D}. To overcome this limitation, the rupture threshold of the elastic-brittle behaviour law has been artificially increased.

2.3 Discrete element modelling

The concrete target slab: The reinforcement pattern is shown in Figure 2. The isotropic and polydisperse packing of 'concrete' elements is obtained through a disorder technique available in *PFC*^{3D}, around the reinforcement lines. A parallel bond was applied between the concrete elements.

Figure 2 The four reinforcement layers of the concrete slab, represented by a set of 17,408 discrete elements (see online version for colours)

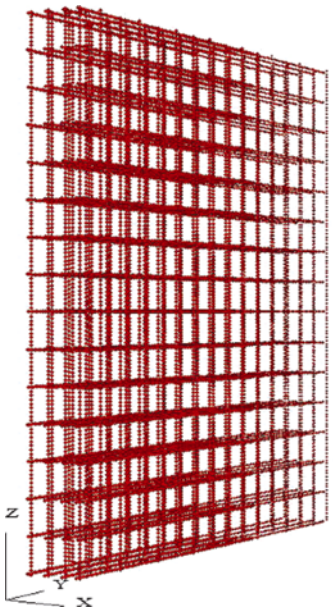

The following procedure was used to set up the model:

1 Generate six walls (a box), which correspond to the edges of the target, i.e. 1.46 × 1.46 × 0.208 m, (as to tests D35 and D37, the box size should be replaced by 1.46 × 1.46 × 0.416 m).

2 Generate the reinforcement elements and set their transition and rotation ability to zero.

3 Generate the concrete elements in an arbitrary way. During this step, all movements between concrete elements are allowed, and the algorithm stops when equilibrium is reached.

4 Set the parallel bonds between all concrete elements, and then delete the front wall and the back wall, which correspond to the impact direction.

5 Release the reinforcement elements.

This procedure is followed to avoid obtaining an undesirable residual contact force between two elements during the DE generation. The total number of Discrete Elements in the concrete slab is 19403, with a radius distribution size between 0.005 m and 0.02 m.

The block: Its geometry is as close as possible to the experimental one. The 'clump' command has been used to simulate the missile, thus all the elements located in this clump can move together as well, so the missile was treated as a rigid body. The diameter and the weight of the missile are kept the same as in the CEA–EDF test, and the local parameters are identical to those of the slab.

Computation conditions: Prior to any computation, gravity is applied on the slab until equilibrium is reached. The block is initially placed just above the slab surface, with the initial velocity corresponding to its impact velocity. The impact configuration (position and orientation) has been set as close as possible to the observed experimental configuration. On each side, a layer of 10 cm is fixed during the calculation. This gives a boundary condition. The block is subjected to gravity as well (Figure 3).

Figure 3 On left, front view of the initial configuration of the impact process, on the right, the side view. Because of the coarse size of the concrete discrete elements, the first reinforcement layer is visible (see online version for colours)

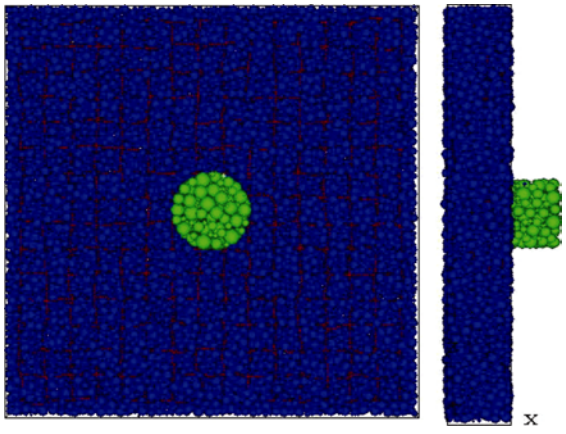

3 Modelling of impact tests

3.1 CEA–EDF tests

The experimental shots were performed by the French Atomic Energy Agency (CEA) and the French Electrical Power Company (EDF) on reinforced concrete slabs,

the thickness of which was chosen to represent, in a realistic way, the thickness of the wall of a reactor containment (Berriaud et al., 1978). Seven tests have been chosen among all the CEA–EDF tests for the numerical simulation. The properties of the concrete material and the geometric shape of the missile (flat nose) were kept constant. The effects of parameters such as the missile velocity (25–450 m/s), its mass (20–300 kg), the ratio of the missile diameter to the thickness of the slab (0.24–2.9) and characteristics of the steel reinforcement were studied (Tables 3 and 4).

Table 3 CEA–EDF tests – concrete slabs

	Concrete slab		*Observation*	
Shot	*Thickness* (m)	*Strength* (MPa)	*Perforation* (*by* PFC^{3D})	*Penetration* (m) (*by equation* (5))
D22	0.208	41.5	Yes	x
D24	0.208	38	No	0.05
D30	0.208	43.5	Yes	x
D27	0.208	44	Yes	x
D28	0.208	43.5	No	0.14
D35	0.416	38.5	No	0.285
D37	0.416	50	Yes	x

Table 4 CEA–EDF tests – missiles

Shot	*Mass* (kg)	*Diameter* (m)	*Velocity* (m/s)	*Momentum* (kgms^{-1})	*Kinetic energy* (kgm^{2}s^{-2})
D22	34	0.278	151	513E+03	388E+05
D24	34	0.278	102	347E+03	177E+05
D30	34.5	0.278	186	642E+03	597E+05
D27	51.6	0.3	129	666E+03	429E+05
D28	32.8	0.3	153	502E+03	384E+05
D35	31	0.3	445	138E+04	307E+06
D37	303	0.1	49	148E+04	3,64E+05

3.2 Numerical results

The results of the tests involving a 1.46×1.46 m concrete slab with a 0.208 m thickness reinforced by four different steel layers, impacted by a 34 kg non-deformable flat-nose missile with a diameter of 0.278 m at velocities of 102, 151 and 186 m/s, were selected to be compared with the numerical model (tests D22, D24, D30). These velocities led to scabbing, penetration and perforation of the slab, respectively.

Gravity is applied to the slab until equilibrium is reached prior to any computation. The block is initially placed just beside the slab surface, with the initial velocity corresponding to its impact velocity. The impact configuration (position and orientation) has been set as close as possible to the observed experimental configuration (Figure 3).

The first results shown were obtained with the simulation of three tests with different impact velocities (102, 151 and 186 m/s, see Figure 4). The other parameters are the same for all three tests. The model can describe the different observed configurations such as perforation, scabbing and penetration.

As soon as the damping factor is set for one of these tests, the model is capable of predicting the trajectory of the missile for the other two cases. Thus, when fixing the damping parameter for the test D22 (151 m/s), which induces penetration and scabbing processes, the model was able to reproduce the slight penetration for the 102 m/s impact velocity and the perforation process for the 186 m/s impact velocity (Figure 5).

Figure 4 Comparisons between simulations and experiments for the three impact velocities: 102, 151 and 186 m/s (see online version for colours)

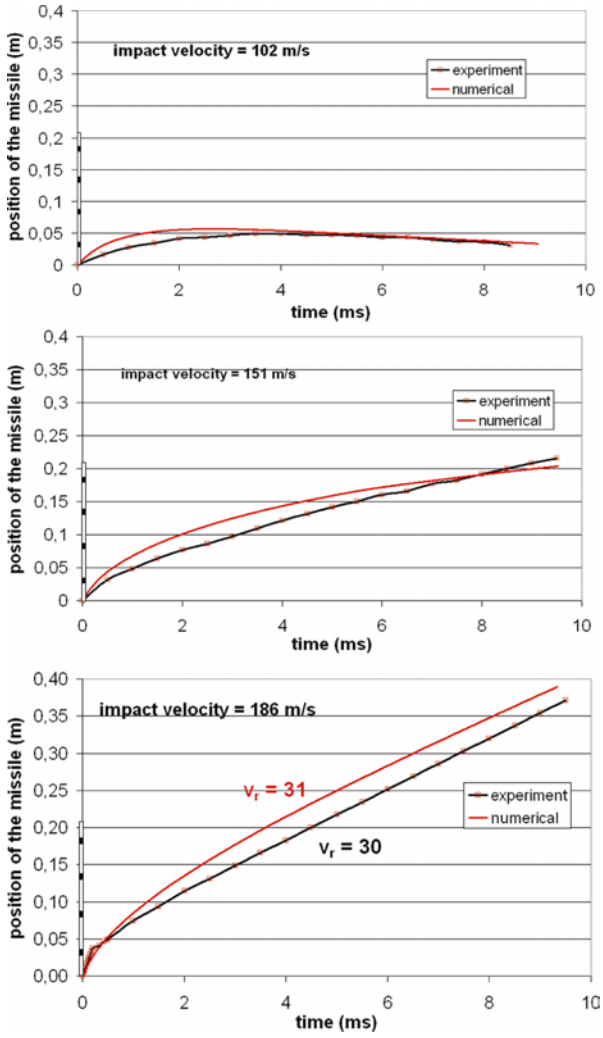

Figure 5 On the left, penetration case for the 102 m/s impact velocity (snap at 8.405 ms); on the right, perforation of the slab for the 186 m/s impact velocity (snap at 9.3 ms). Both cases are observed in experiments for the same impact velocity (see online version for colours)

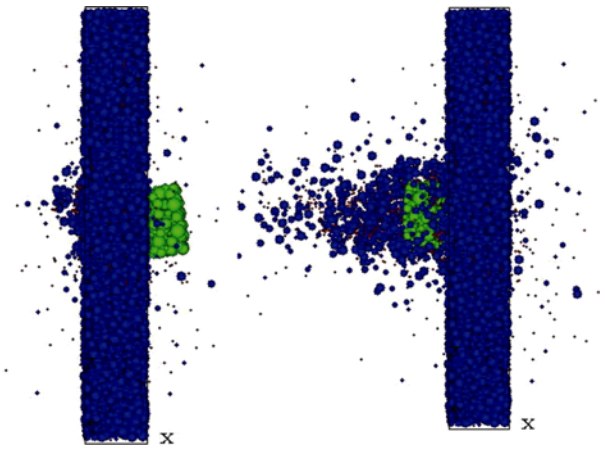

The penetration depth was also calculated after numerical simulation for tests involving a simple penetration (no perforation had occurred; test D22, D28, D35), because these penetration test data are difficult to obtain, our numerical penetration results have been compared with the penetration prediction formula proposed by Li and Tong (2003), which has been deemed reliable in recent years.

$$\frac{X}{D} = \sqrt{\frac{(1+k\pi/4N)}{(1+I_d/N_d)}\frac{4k}{\pi}I_d}, \quad \text{for } \frac{X}{D} \le k \tag{5a}$$

$$\frac{X}{D} = \frac{2}{\pi}N_d \ln\left[\frac{1+I_d/N_d}{1+k\pi/4N_d}\right] + k \quad \text{for } \frac{X}{D} > k \tag{5b}$$

where X is the penetration depth, D is the diameter of the missile, k is the dimensionless penetration depth, as a flat-nose missile is used here, k is equal to 0.707, and two dimensionless numbers: the impact function I_d and the geometry function N_d, which are defined as $I_d = (Mv^2/D^3 f_c)/\left(82.6 f_c^{-0.544}\right)$, $N_d = M/(\rho_c D^3)$ for a flat-nose missile, where M is the mass of the missile, ρ_c is the density of a concrete target, v is the impact velocity and f_c is the compressive stress of a concrete target.

Li and Tong (2003) has also proposed a prediction formula for a small penetration depth, i.e., when $X/D < 0.5$ the following equation should be used,

$$\frac{X_{\text{test}}}{D} = 1.628\left(\frac{X_{\text{anal}}}{D}\right)^{2.789}. \tag{5c}$$

The numerical results show a good agreement with equation (5) (where equation (5c) was used for test D24, see Table 3). This is true up to test D35, which involves a thicker target (0.416 m). This could be due to the lack of plasticity in the reinforcement as well as the fact that ductility is not imposed in the concrete used in the numerical model. All in all, the difference between the numerical results and the prediction formula for test D35 is about 20%.

After having identified the local parameters as explained previously and calibrated the damping parameter with the 151 m/s impact velocity test, some other tests were studied to analyse the influence of reinforcement and other parameters of the empirical formulae.

3.3 *Influence of reinforcement ratio*

The influence of the reinforcement ratio was analysed and compared with an empirical formula derived from Berriaud et al. (1978) and modified by the United Kingdom Atomic Energy Authority (Fullard et al., 1991):

$$v_p = 1.3\rho_c^{1/6} f_c^{1/2} (D d_p^2/M)^{2/3} (r+0.3)^{0.5} \tag{6}$$

in which SI units are required. v_p (m/s) is the ballistic limit, ρ_c is the density of the concrete, f_c is the compressive strength of concrete, D is the missile diameter (flat nose), d_p is the slab thickness, M is the missile mass and r is the reinforcement ratio.

To change the reinforcement ratio in the numerical simulation instead of changing the diameter of an element, the yield stress of the parallel bond of all reinforcement elements has been increased (pb_nstrength, pb_sstrength). Thus, the effect of increasing the resistance of rebars is equivalent to increase the reinforcement ratio. The advantage of this procedure is that we can avoid a complicated element-generating step as described in Section 2.3.

Equation (5) gives the correct prediction of perforation for tests D22 and D30. Figure 6 shows the influence of the reinforcement ratio on the penetration of the missile. There is no influence of the reinforcement ratio on the penetration depth since the initial velocity of the missile is much lower than the ballistic limit velocity. Also, note that equation (5) predicts a perforation for a 102 m/s impact test and for a reinforcement ratio lower than 0.35%, which is in opposition to the simulation results.

Figure 6 Influence of reinforcement ratio on missile position for tests D24 (102 m/s), D22 (151 m/s) and D30 (186 m/s) (numerical) (see online version for colours)

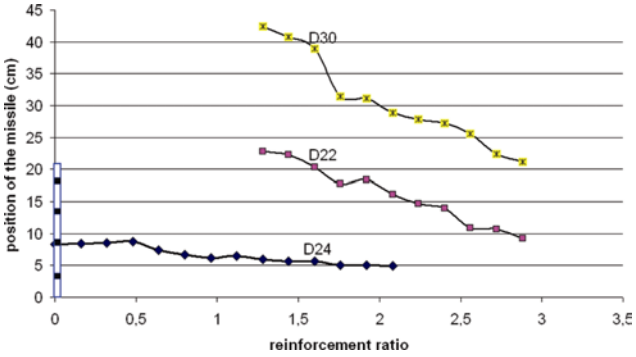

Tests D22 and D28 were also analysed since they differ slightly but the perforation occurred only for test D22. Equation (5) predicts that there is no penetration in either test (Figures 7 and 8) while the numerical simulation, on the other hand, correctly predicted the perforation.

Figure 7 Influence of reinforcement ratio on missile position for tests D22 and D28 (according to equation (1)) (see online version for colours)

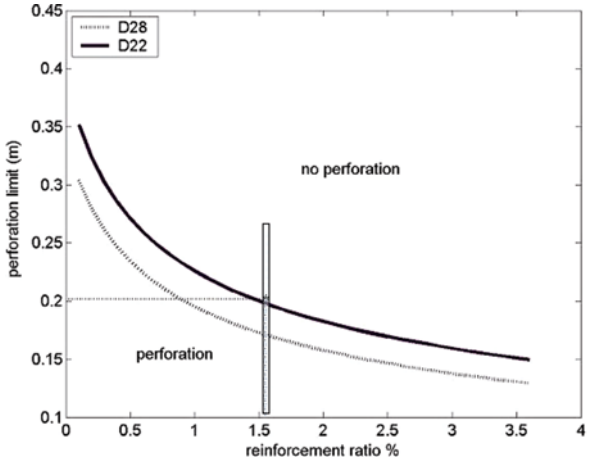

Figure 8 Influence of reinforcement ratio on missile position for tests D22 and D28 (numerical) (see online version for colours)

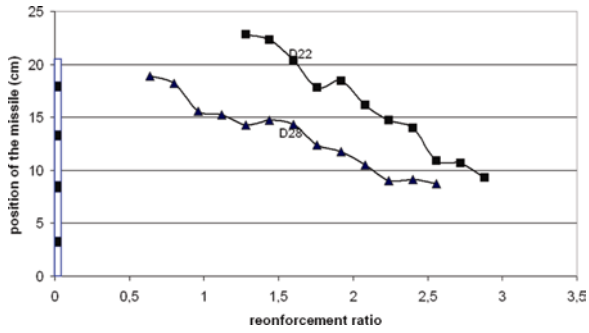

Figure 9 shows the images captured after impact. The impact time duration was the same for all simulations. The penetration degrees for the different reinforcement ratios are easily distinguishable.

Figure 9 Influence of reinforcement ratio on the final missile position for test D22 (151 m/s), the perforation occurs for a reinforcement ratio <2.24% (see online version for colours)

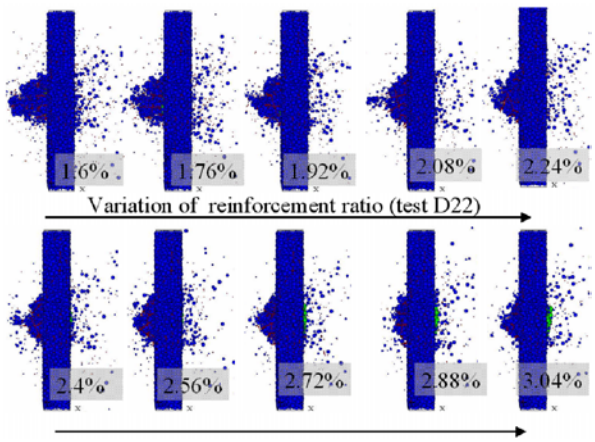

The concrete and the reinforcement elements were bonded together with parallel bonds (PFC^{3D}, 2003). To analyse the damage between the discrete elements after impact, the percentage of broken bonds given by the numerical modelling has been calculated and shown in Figure 10. Considering that the target's surrounding is less damaged, we can concentrate on the impact zone, which was considered as a square area around the impact point (as shown in Figure 10). Serious damage was observed: the broken bonds of the rebars in this zone can vary considerably from 50% to 20%. Thus, for test D22, if the reinforcement ratio is increased to a certain percentage, the target can be well protected from missile penetration.

In test D35, one may observe that the final position of the missile can be separated into two parts depending on the reinforcement ratio. While the reinforcement ratio is less than 2%, the final position of the missile will be dominated seriously by the reinforcement, while the other part will not. This observation agrees with the empirical formulae, that is to say, the reinforcement will play an important role when the missile attempts to perforate the target. On the other hand, when the missile can easily penetrate the target, the influence of reinforcement can be ignored. This is why in recent empirical perforation formulae, the reinforcement is often considered within the ballistic limit.

Prior to the current work, there was little information about the effect of the reinforcement ratio in a concrete target during a missile impact. The numerical approach makes it possible to study this parameter. According to our numerical simulations, the reinforcement could play an important role when the target tends to be perforated.

Figure 10 Influence of reinforcement ratio on percentage of broken bonds for test D22, in global assessment and central assessment (see online version for colours)

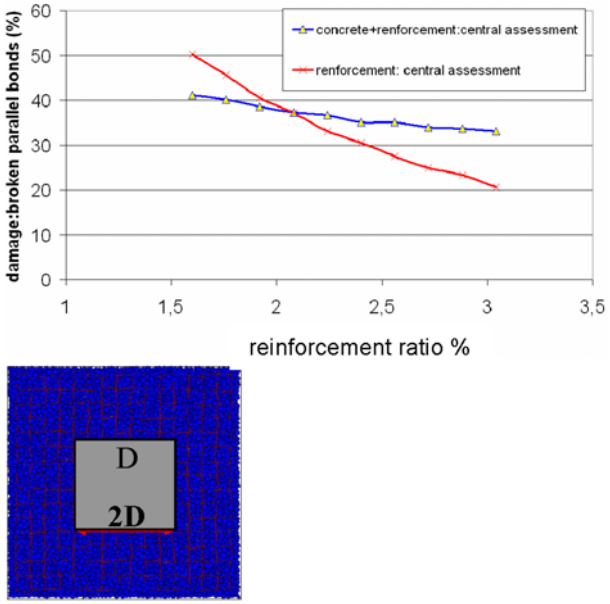

3.4 Kinetic energy and momentum

Tests D35 and D37 are close in terms of momentum, but test D35 corresponds to a much higher kinetic energy. The discrete element model could correctly predict the

perforation and penetration phenomena for both tests whereas equation (5) could not. The numerical results and the result predicted by equation (5) are shown in Figures 11 and 12. As shown in Figure 11, the two tests are very close. This means that considering two missiles, one with a low weight and high velocity (D35), and the other with a high weight and low velocity (D37), the two tests should have similar perforation behaviour. According to experimental results, only D37 is perforated, which is well reproduced in the numerical model (Figure 12). Some phenomena were noted during the numerical simulation: the impact energy of test D35, which involves a significant diameter (0.3 m), was dissipated quickly by the friction between the missile and concrete elements resulting in a sharp decrease in the impact velocity. As to test D37, which involves a small diameter, it is easier for the missile to perforate the target. When the missile is first launched, scabbing occurs; then, if the missile has a high enough remaining velocity, the complete perforation of the target takes place. Therefore, momentum and kinetic energy are not sufficient parameters to predict the perforation of concrete slabs.

Figure 11 Influence of reinforcement ratio on missile position for tests D35 and D37 (according to equation (1)) (see online version for colours)

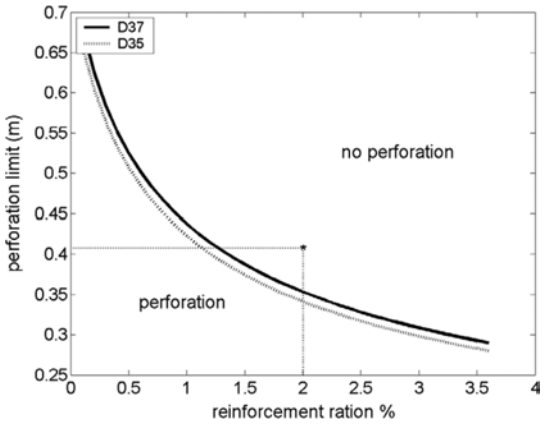

Figure 12 Influence of reinforcement ratio on missile position for tests D35 and D37 (numerical)

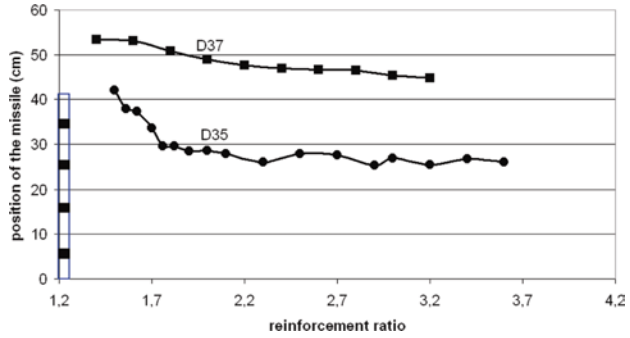

4 Conclusion

The main specificities of the 3D Discrete Element approach are the following: the modelling scale is higher than the heterogeneity scale, so the model may be used to simulate real structures, which means that the DEM is mainly used here for its ability to treat discontinuities; the interaction laws introduced are then very simple and are close to macroscopic laws; finally, an identification process based on quasi-static tests is used, so the quasi-static behaviour of concrete is reproduced. This identification process is the key point, to allow a complete predictive computation.

In this work, the CEA–EDF impact tests were studied and simulated with this model, for different impact velocities, on a reinforced concrete slab at a real scale. Results were compared with experimental results: quantitatively results are very coherent with respect to experimental results. Moreover, using parametric studies, the numerical model has given interesting insights on the role of the reinforcement during the perforation process in a better way than the classical predictive empirical formulations. The numerical simulation results have shown that the reinforcement ratio has little influence on the penetration depth since the impact velocity is not close to the ballistic limit to perforate the target. On the other hand, the reinforcement ratio has a strong influence on the missile residual velocity and on damage in concrete in the case of perforation.

References

Berriaud, C., Sokolovsky, A., Gueraud, R., Dulac, J. and Labrot, R. (1978) 'Local behavior of reinforced concrete walls under missile impact', *Nuclear Engineering and Design*, Vol. 45, No. 2, pp.457–469.

Camborde, F., Mariotti, F. and Donzé, F.V. (2000) 'Numerical study of rock and concrete behavior by discrete element modelling', *Computers and Geotechnics*, Vol. 27, No. 4, pp.225–247.

Cundall, P.A. and Strack, O.D.L. (1979) 'A discrete numerical model for granular assemblies', *Géotechnique*, Vol. 29, No. 1, pp.47–65.

Degen, P.P. (1980) 'Perforation of reinforced concrete slabs by rigid missiles', *ASCE Journal of the Structural Division*, Vol. 106, No. 7, pp.1623–1642.

Donzé, F.V. and Magnier, S-A. (1997) *Spherical discrete element code*, Discrete Element Project Report no. 2, GEOTOP, Université du Québec à Montréal.

Fullard, K., Baum, M.R. and Barr, P. (1991) 'The assessment of impact on nuclear power plant structures in the United Kingdom', *Nuclear Engineering and Design*, Vol. 130, No. 2, pp.113–120.

Hentz, S., Daudeville, L. and Donzé, F.V. (2004a) 'Identification and validation of a discrete element model for concrete', *Journal of Engineering Mechanics*, Vol. 130, No. 6, pp.709-719.

Hentz, S., Daudeville, L. and Donzé, F.V. (2004b) 'Discrete element modelling of concrete submitted to dynamic loading at high strain rates', *Computers and Structures*. Vol. 82, Nos. 29–30, pp.2509–2524.

Hughes, G. (1984) 'Hard missile impact on reinforced concrete', *Nuclear Engineering and Design*, Vol. 77, No. 1, pp.23–35.

Iwashita, K. and Oda, M. (2000) 'Micro-deformation mechanism of shear banding process based on modified distinct element method', *Powder Technology*, Vol. 109, pp.192–205.

Li, Q.M. and Tong, D.J. (2003) 'Perforation thickness and ballistic limit of concrete target subjected to rigid projectile impact', *Journal of Engineering Mechanics*, Vol. 129, No. 9, pp.1083–1091.

Li, Q.M., Reid, S.R., Wen, H.M. and Telford, A.R. (2006) 'Local impact effects of hard missiles on concrete targets', *International Journal of Impact Engineering*, Vol. 32, Nos. 1–4, pp.224–284.

Magnier, S-A. and Donzé, F.V. (1998) 'Numerical simulations of impacts using a discrete element method', *Mechanics of Cohesive-Frictional Materials*, Vol. 3, No. 3, pp.257–276.

Masuya, H., Kajikawa, Y. and Nakata, Y. (1994) 'Application of the distinct element method to the analysis of the concrete members under impact', *Nuclear Engineering and Design*, Vol. 150, Nos. 2–3, pp.367–377.

Meguro, K. and Hakuno, M. (1989) 'Fracture analyses of concrete structures by the modified distinct element method', *Structural Engineering/Earthquake Engineering*, Vol. 6, No. 2, pp.283–294.

Particle Flow Code in 3 Dimensions (PFC^{3D}) (2003) *Version 3.0*, Itasca Consulting Group Inc., Minneapolis, Minnesota.

Potapov, A.A., Hopkins, M.A. and Campbell, C.S. (1995) 'A two-dimensional dynamic simulation of solid fracture part I: description of the model', *International Journal of Modern Physics*, Vol. 6, No. 3, pp.371–398.

Potyondy, D.O., Cundall, P.A. and Lee, C.A. (1996) 'Modelling rock using bonded assemblies of circular particles, in rock mechanics tools and techniques', *Proc. Second North American Rock Mechanics Symposium*, Montréal, June, pp.1937–1944

Riera, J.D. and Iturrioz, I. (1998) 'Discrete elements model for evaluating impact and impulsive response of reinforced concrete plates and shells subjected to impulsive loading', *Nuclear Engineering and Design*, Vol. 179, No. 2, pp.135–144.

Shiu, W, Donzé, F.V. and Daudeville, L. (2008a) 'Penetration prediction of missiles with different nose shapes by the discrete element numerical approach', *Computers and Structures*, Vol. 86, Nos. 21–22, pp.2079–2086.

Shiu, W, Donzé, F.V. and Daudeville, L. (2008b) 'Compaction process in concrete during missile impact: a DEM analysis', *Computers and Concrete*, Vol. 5, No. 4, pp.329–342.

Williams, M.S. (1994) 'Modeling of local impact effects on plain and reinforced concrete', *ACI Structural Journal*, Vol. 91, No. 2, pp.178–187.

Nomenclature

$A_{(i)}$	Generalised acceleration
D	Diameter of the missile
d_p	Slab thickness
E_c	Young's modulus of the concrete
E_s	Young's modulus of the steel reinforcement
F_i	*i*th component of the generalised contact force
$F_{(i)}^d$	Damping force
f_c	Compressive stress of a concrete target
g	Gravitational acceleration
I	Moment of inertia
I_d	Impact function $(= (Mv^2 / D^3 f_c)/(82.6 f_c^{-0.544}))$
J	Polar moment of the disk's cross-section (between two bonding elements)
K_i	*i*th component of the element stiffness
kn	Normal stiffness of the element
$\overline{k}^n$	(also noted Pb_kn) the normal stiffness of the parallel bond
ks	Tangent stiffness of the element
$\overline{k}^s$	(also noted Pb_ks) the tangent stiffness of the parallel bond
k	Dimensionless penetration depth
M	Mass of the missile
M_i	Generalised moment acting on each element
$\overline{M}_i^n$	Normal generalised moment acting on each parallel bond
$\overline{M}_i^s$	Tangent generalised moment acting on each parallel bond
m	Mass of the element
N_d	Geometry function $(= \mathrm{M}/(\rho_c D^3))$
Pb_nstrength	Parallel bond maximum normal stress
Pb_sstrength	Parallel bond maximum shear stress
r	Reinforcement ratio
U_i	Overlap between two elements in contact
v	Impact velocity
v_p	Ballistic limit
X	Penetration depth
$\ddot{x}_i$	Translation acceleration
Greek symbols	
α	Numerical damping factor
μ	Friction coefficient
$\Delta\theta^n$	Normal relative angular rotation between two elements in contact
$\Delta\theta^s$	Tangent relative angular rotation between two elements in contact
$\dot{\omega}_i$	Rotational acceleration
ρ_c	Density of a concrete target